Environmental Science & Technology Letters

pubs.acs.org/journal/estlcu

Letter

Process-Level Quantification on Opposite $PM_{2.5}$ Changes during the COVID-19 Lockdown over the North China Plain

Lei Chen, Hong Liao,* Ke Li, Jia Zhu, Ziyu Long, Xu Yue, Yang Yang, and Meigen Zhang

Cite This: *Environ. Sci. Technol. Lett.* 2023, 10, 779−785

Read Online

ACCESS | Metrics & More | Article Recommendations | Supporting Information

ABSTRACT: By using an improved process-level quantification method implemented in the WRF-Chem model, we provide a quantitative analysis on contribution of each physical/chemical process to $PM_{2.5}$ change from before to during the COVID-19 lockdown and further identify a dominant process responsible for inverse $PM_{2.5}$ changes over the southern and northern North China Plain (NCP). From before to during the lockdown period, the $PM_{2.5}$ concentration over the southern NCP decreased by 61.0 $\mu g\ m^{-3}$; a weakened aerosol chemistry production process mainly resulting from emission mitigation of precursors was identified to be the leading process for the $PM_{2.5}$ decrease. However, the northern NCP suffered from an unexpected $PM_{2.5}$ increase of 10.0 $\mu g\ m^{-3}$, which was primarily attributed to a weakened advection dilution process induced by decreased wind speed. The improved process analysis method, superior to the traditional one, can be applied to any two periods rather than two instantaneous time points, and therefore it exerts a new contribution to understand the pollution evolution mechanism from a process-level quantitative perspective.

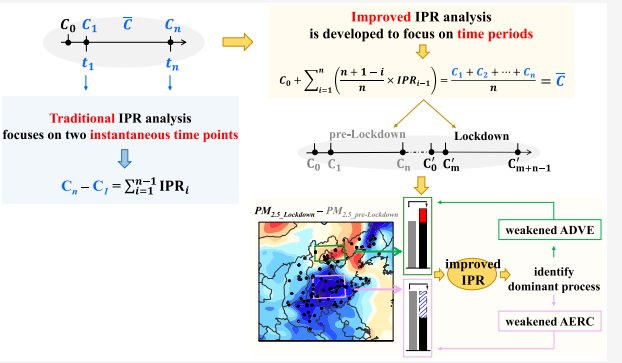

KEYWORDS: *$PM_{2.5}$, improved process analysis, opposite change, WRF-Chem, North China Plain*

INTRODUCTION

In early 2020, China implemented nationwide restrictions on human activities to prevent the spread of Coronavirus Disease 2019 (COVID-19). Benefitting from effective emission reduction measures (e.g., a moratorium on industrial and transportation activities), large reductions in sulfur dioxide (SO_2) and nitrogen oxide (NO_x) were generally observed.[1,2] Although primary pollutants drastically decreased during the COVID-19 lockdown period, haze pollution still occurred over some regions of eastern China.[3−5] Parts of the North China Plain (NCP) even suffered from worse $PM_{2.5}$ air quality compared with the pre-lockdown period.[6,7]

Heavy haze pollution accompanied by countrywide reduction in anthropogenic emissions seeded doubt among the public about the effectiveness of clean air actions and thus triggered academic discussions on the reasons for haze pollution or $PM_{2.5}$ increases during the COVID-19 lockdown. Possible reasons reported by previous studies included unfavorable meteorological conditions which offset the benefits of emissions reduction,[8,9] enhanced secondary aerosol formation due to increased oxidation capacity,[7,10] and promotion of aerosol heterogeneous chemistry owing to anomalously high humidity.[10] Despite the above reasons, quantification on each factor's contribution and identification of the leading reason remain scarce, which calls for further quantitative analysis.

Evolution of $PM_{2.5}$ pollution is the combined result of various physical and chemical processes. Process-level analysis technique, i.e., integrated process rate (IPR) analysis, can be applied to air quality models to separate individual contributions of each physical/chemical process to variations in $PM_{2.5}$ concentrations.[11,12] Following the definition of process analysis by Gipson,[13] traditional IPR analysis is widely used to quantify process contributions to concentration differences between two instantaneous time points[14−18] (e.g., hourly changes from the previous hour to the current hour, 24-h changes from 0:00 to 23:00).

However, in more cases, what we are concerned with is not the process contribution to concentration difference between two instantaneous time points (e.g., the concentration at 00:00 January 1, 2013 vs the concentration at 23:00 December 31, 2020) but rather the process contribution to mean concentration difference between two time periods (e.g., the impact of each process on decreased/increased $PM_{2.5}$/ozone concentrations from year 2013 to year 2020). Clearly,

Received: July 11, 2023
Revised: August 26, 2023
Accepted: August 28, 2023
Published: August 30, 2023

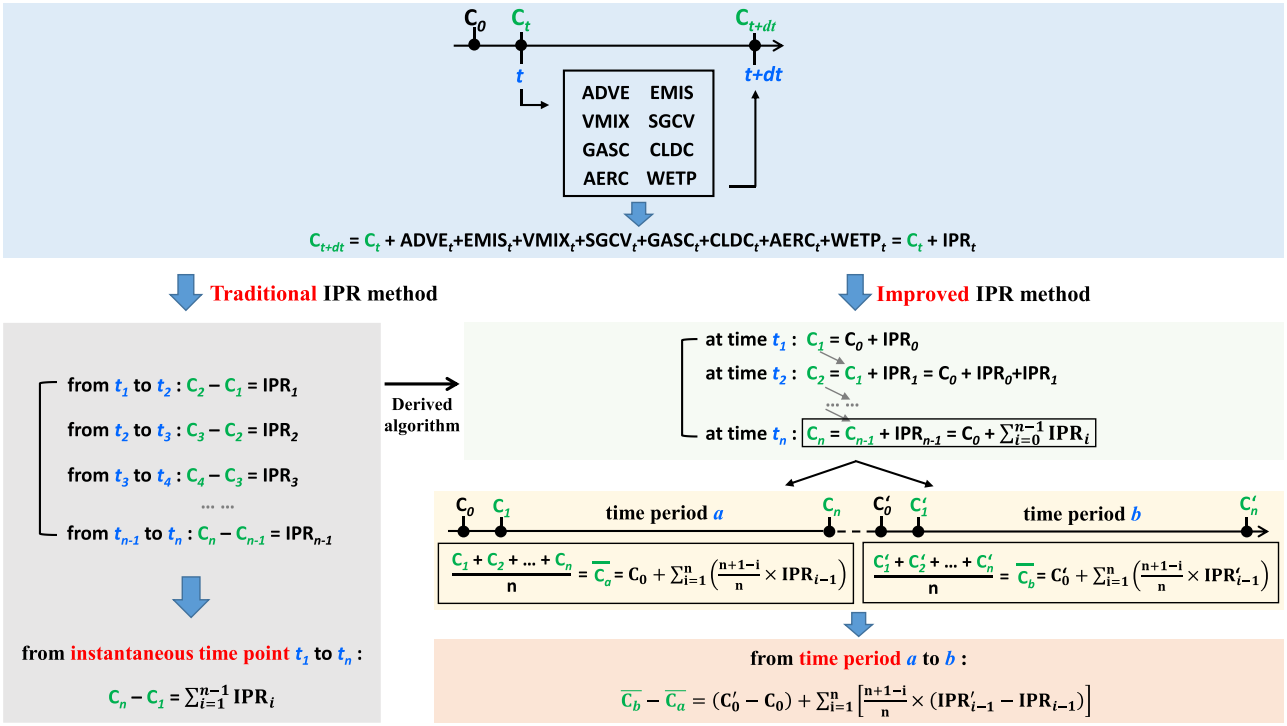

Figure 1. Simplified schematic diagram of the traditional and improved integrated process rate (IPR) analysis method. ADVE, EMIS, VMIX, SGCV, GASC, CLDC, AERC, and WETP represent advection, primary emission, vertical mixing, subgrid convection, gas-phase chemistry, cloud chemistry, aerosol chemistry, and wet scavenging process, respectively. C_0 and C_0' are initial concentrations. C_n and C_n' mean concentrations at time point t_n. dt is the time step. IPR_n and IPR_n' mean the combined effects of all physical and chemical processes at time point t_n, which can be separated to individual contribution of each process. $\overline{C_a}$ and $\overline{C_b}$ represent the averaged concentrations during period a and b.

conclusions based on the mean concentration difference between two time periods are more robust and strengthen research significance, providing more useful suggestions for air pollution control. However, no previous studies have optimized the conventional IPR to examine process contribution to concentration differences between two time periods.

Here we quantified the contribution of each physical/chemical process to $PM_{2.5}$ changes from the pre-lockdown period to the lockdown period and further identified the dominant process responsible for the $PM_{2.5}$ change, by using an improved process-level quantification method implemented in WRF-Chem. Particularly, this paper applied the improved IPR to the southern and northern NCP to account for the inverse $PM_{2.5}$ changes over the two regions. The improved process analysis method can be applied to any two periods to quantify process contributions to changes in pollutant concentrations, and therefore it exerts a novel contribution to understand the mechanism of air pollution variation from a process-level quantitative perspective.

MATERIALS AND METHODS

Model Configuration. The Weather Research and Forecasting with Chemistry model (WRF-Chem) was used to investigate $PM_{2.5}$ variations in NCP before (January 1 to 21, 2020, denoted as "pre-lockdown") and during (January 24 to February 13, 2020, denoted as "lockdown") the COVID-19 lockdown. Anthropogenic emissions during the pre-lockdown and lockdown periods were adopted from Huang et al.[7] and Zheng et al.[19] As shown in Figure S1, emissions of major $PM_{2.5}$ precursors during the lockdown were decreased by 15.0−45.0% compared with those during pre-lockdown, except for limited changes in NH_3 emissions. More detailed model configurations and parametrizations are described in Text S1 and Table S1.

Improved Integrated Process Rate (IPR) Analysis. Using a numerical technique of operator splitting, Eulerian models solve the continuity equation in several simple ordinary or partial differential equations representing the impact of a certain process;[20,21] therefore, the contribution of each physical/chemical process to variations in simulated pollutant concentrations at each time step (i.e., concentration difference between current- and previous-time step) can be diagnosed by a method named IPR analysis. A detailed introduction to IPR was described in Gipson[13] and Chen et al.[16] Following the definition of IPR, this method was conventionally applied to assess contributions of physical/chemical processes to concentration differences between two instantaneous time points, e.g., hourly (current hour relative to previous one) changes, 24-h (23:00 relative to 0:00) changes, and even more general changes from instantaneous time point t_1 to t_n (light gray box in Figure 1).[11,12,14−18,22−26]

Due to the limitation of conventional IPR which quantifies the process contribution to concentration variation between two instantaneous time points, we extend the applicability scope of IPR. The improved IPR can quantify the impact of each process on the mean concentration averaged over any time period (light orange box in Figure 1) and calculate the process contribution to the mean concentration difference between any two time periods (light red box in Figure 1). Detailed documentation of specific improvement steps for the improved IPR can be found in Text S2. It is noted that the essential attributes of traditional IPR and the improved one are the same. The improved IPR is derived from the traditional

https://doi.org/10.1021/acs.estlett.3c00490
Environ. Sci. Technol. Lett. 2023, 10, 779−785

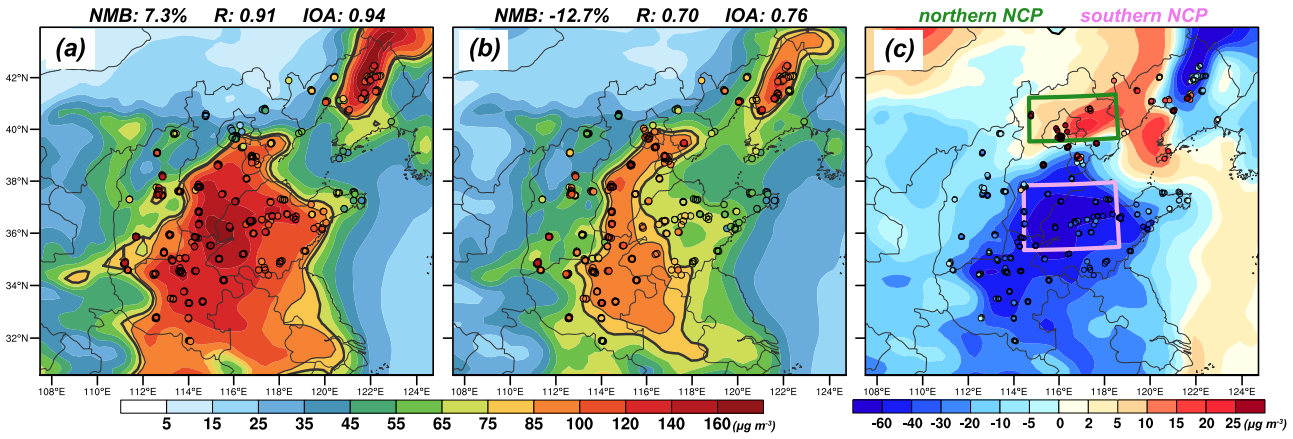

Figure 2. Spatial distributions of observed (circles) and simulated (shades). (a) $PM_{2.5}$ concentrations before the COVID-19 lockdown, (b) $PM_{2.5}$ concentrations during the COVID-19 lockdown, and (c) $PM_{2.5}$ changes from before to during the COVID-19 lockdown. The normalized mean bias (NMB), correlation coefficient (R), and index of agreement (IOA) between daily sites-averaged measurements and simulations are also shown at the top of each panel. The black contour lines in (a) and (b) represent National Ambient Air Quality Standard grade II limit value for daily $PM_{2.5}$ concentrations (i.e., 75 μg m^{-3}). The green/pink box in (c) represents the northern/southern North China Plain with the largest $PM_{2.5}$ increases/decreases.

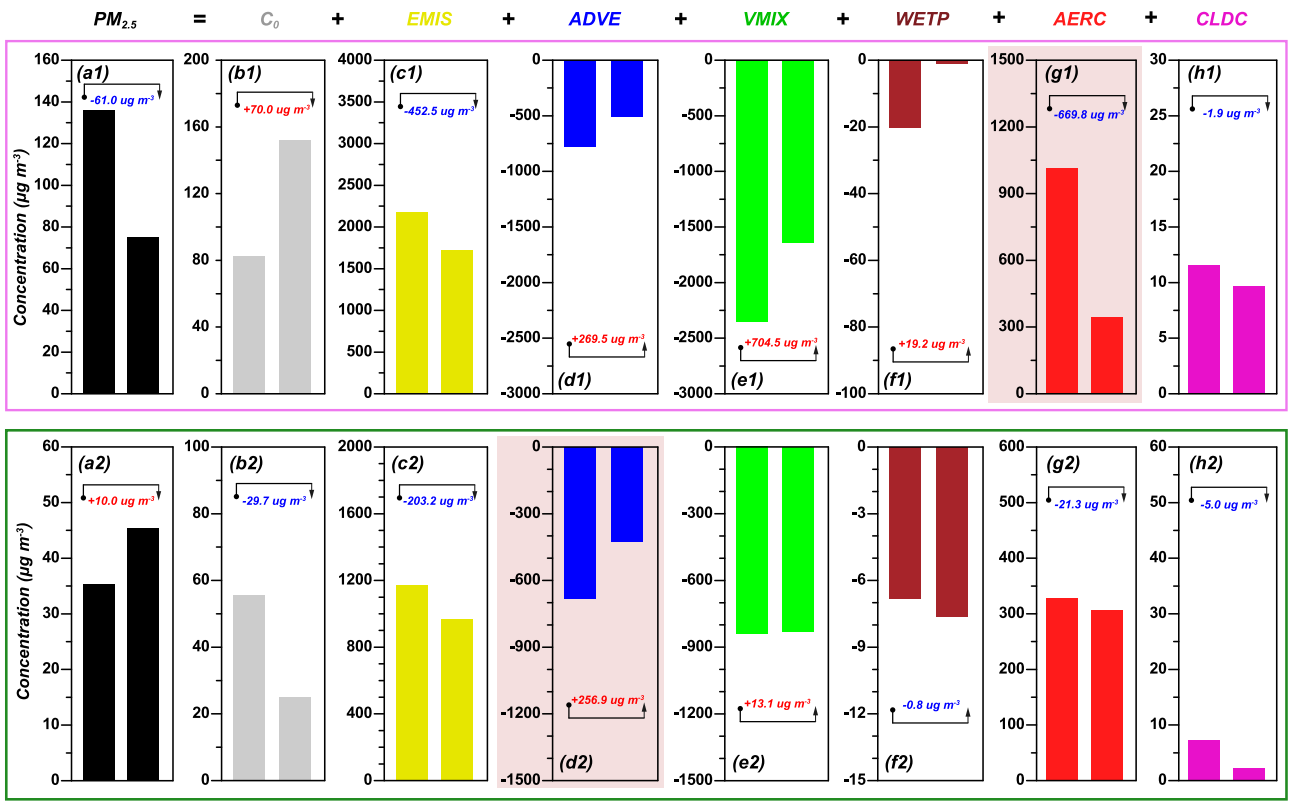

Figure 3. (a1−a2) Simulated $PM_{2.5}$ concentrations represented by the combined effects of (b1−b2) initial concentration (C_0), (c1−c2) EMIS, (d1−d2) ADVE, (e1−e2) VMIX, (f1−f2) WETP, (g1−g2) AERC, and (h1−h2) CLDC process averaged during the pre-lockdown period (left bar) and lockdown period (right bar) over the southern (top purple box) and northern (bottom green box) North China Plain. The $PM_{2.5}$ changes contributed by each process from the pre-lockdown period to the lockdown period are shown in positive or negative values in each panel. The contributions of SGCV and GASC processes are not shown due to their negligible impact.

method. The key improvement and uniqueness of the improved approach is the wider applicability because none of previous studies quantified the process contribution to mean concentration differences between two time periods with the traditional method. Text S3 and Figure S2 detailedly compare the differences in application between the traditional and improved IPR methods.

Involved physical/chemical processes in WRF-Chem include advection (ADVE), primary emission (EMIS), vertical mixing (dry deposition and turbulent diffusion) (VMIX), subgrid convection (SGCV), gas-phase chemistry (GASC), cloud chemistry (CLDC), aerosol chemistry (AERC), and wet scavenging (WETP). It is noted that "primary emission" here refers to primary emission of $PM_{2.5}$, excluding emissions of $PM_{2.5}$ precursors (e.g., SO_2). The impacts of precursor

https://doi.org/10.1021/acs.estlett.3c00490
Environ. Sci. Technol. Lett. 2023, 10, 779−785

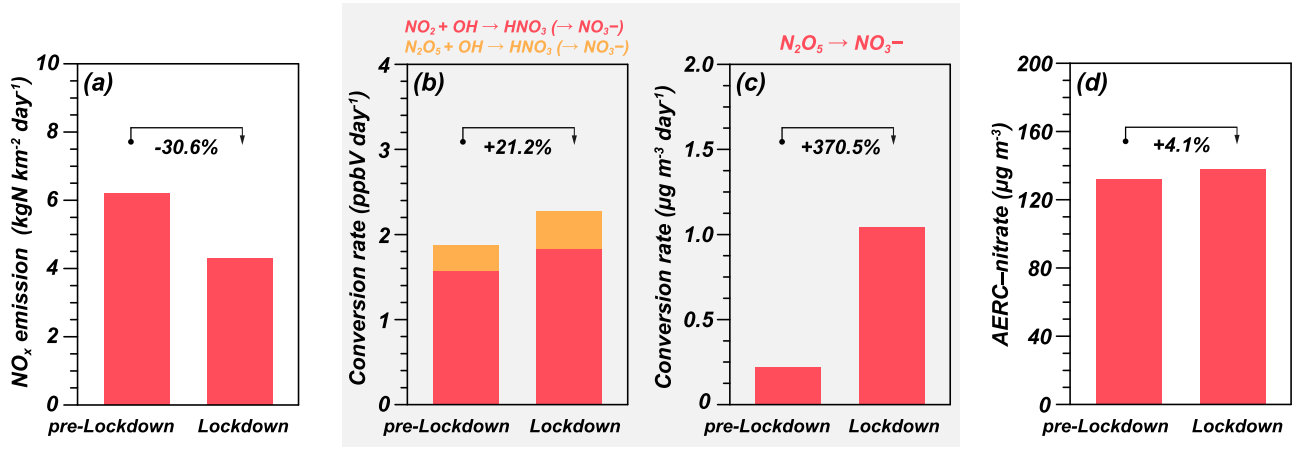

Figure 4. (a) Anthropogenic NO_x emissions, (b) chemical conversion rates of gas-phase reactions of OH with NO_2 and N_2O_5 to generate HNO_3, (c) chemical conversion rates of heterogeneous reaction of N_2O_5 on particle surface to generate nitrate, and (d) nitrate concentrations contributed by AERC process (AERC-nitrate), averaged over the northern North China Plain during pre-lockdown and lockdown periods. Respective percentage changes from pre-lockdown to lockdown are also shown in each panel. The HNO_3 formed by gas-phase reactions of OH with NO_2 and N_2O_5 are further converted to particulate nitrate, which is included in the AERC process.

emission on $PM_{2.5}$ by secondary conversion are embodied in chemical processes, rather than a primary emission process.

This paper applied the improved IPR to pre-lockdown and lockdown periods, respectively, aiming to quantify contributions of each physical/chemical process to $PM_{2.5}$ concentrations averaged over both periods and further identify the dominant process for $PM_{2.5}$ changes from pre-lockdown to lockdown. We conducted improved IPR for both southern and northern NCP, trying to quantitatively explain opposite $PM_{2.5}$ changes over the two regions.

Observational Data. Observed meteorological variables were available at Wyoming Weather Web (http://weather.uwyo.edu/surface/meteorogram/seasia.shtml). Monitoring data of $PM_{2.5}$ concentrations were obtained from China National Environmental Monitoring Center (CNEMC, https://quotsoft.net/air/). Measurements of $PM_{2.5}$ compositions and oxidant hydroxyl radical (OH) were collected from refs 29, 35, 37−42. The oxidant O_x was calculated by O_3 and NO_2 ($O_X = O_3 + NO_2$); the O_3 and NO_2 concentrations were taken from CNEMC.

RESULTS AND DISCUSSION

Model Evaluation. We conducted a detailed model evaluation in Text S4. In general, the WRF-Chem model successfully captured the evolutions of observed meteorological parameters (Figures S3−S5), $PM_{2.5}$ levels (Figures S6−S7), $PM_{2.5}$ compositions (Figure S8), and oxidant O_x (Figure S9), as well as the changes from the pre-lockdown to lockdown period in $PM_{2.5}$ levels (Figure 2), $PM_{2.5}$ compositions (Tables S2−S4), and oxidant OH (Figure S10).

Sharp Contrasts in $PM_{2.5}$ Changes over Southern versus Northern NCP. Figure 2 shows simulated $PM_{2.5}$ concentrations before and during COVID-19 lockdown periods. Severe haze pollution swept across southern NCP during pre-lockdown, with $PM_{2.5}$ concentrations exceeding National Ambient Air Quality Standard (i.e., 75 $\mu g\ m^{-3}$) over almost the whole southern NCP (Figure 2(a)). During lockdown, the intensity and extent of $PM_{2.5}$ pollution became much smaller (Figure 2(b)), compared to those during pre-lockdown. We further exhibited $PM_{2.5}$ changes from pre-lockdown to lockdown (Figure 2(c)) and found completely opposite $PM_{2.5}$ changes, i.e., expected $PM_{2.5}$ decreases over southern NCP and unexpected $PM_{2.5}$ increases over northern NCP.

The inverse $PM_{2.5}$ changes as a result of nationwide emission reduction went beyond our understanding. We further focused our attention on the two regions with the largest $PM_{2.5}$ decreases (pink box in Figure 2(c)) and increases (green box in Figure 2(c)). Simulated $PM_{2.5}$ changes from pre-lockdown to lockdown were −61.0 $\mu g\ m^{-3}$ and +10.0 $\mu g\ m^{-3}$ averaged over the two regions. We applied the improved IPR to the two regions to identify the leading process responsible for the respective $PM_{2.5}$ changes.

Key Processes Driving Opposite $PM_{2.5}$ Changes. Over southern NCP, the $PM_{2.5}$ concentration was decreased by 61.0 $\mu g\ m^{-3}$ from pre-lockdown to lockdown (Figure 3(a1)). Compared with pre-lockdown, the lockdown period suffered from a higher initial concentration (C_0) and weaker physical dilution including advection (ADVE), vertical mixing (VMIX), and wet scavenging (WETP), which caused $PM_{2.5}$ increases of 70.0 $\mu g\ m^{-3}$ (Figure 3(b1)), 269.5 $\mu g\ m^{-3}$ (Figure 3(d1)), 704.5 $\mu g\ m^{-3}$ (Figure 3(e1)), and 19.2 $\mu g\ m^{-3}$ (Figure 3(f1)), respectively. The improved $PM_{2.5}$ air quality was driven by weakened aerosol chemical production (AERC in Figure 3(g1)), followed by reduced primary emission (EMIS in Figure 3(c1)) and weakened cloud chemical production (CLDC in Figure 3(h1)). The contributions of subgrid convection (SGCV) and gas-phase chemistry (GASC) processes were not shown due to their negligible impacts. AERC, EMIS, and CLDC processes contributed −669.8 $\mu g\ m^{-3}$, −452.5 $\mu g\ m^{-3}$, and −1.9 $\mu g\ m^{-3}$, respectively, to $PM_{2.5}$ decreases. Therefore, the weakened aerosol chemical production process, which mainly resulted from emission mitigation of aerosol precursors (e.g., SO_2 and NO_x, Figure S1), was identified to be the primary process responsible for the $PM_{2.5}$ decrease over southern NCP, as expected.

We paid more attention to the northern NCP which suffered from an unexpected $PM_{2.5}$ increase. From pre-lockdown to lockdown, the $PM_{2.5}$ concentration was increased by 10.0 $\mu g\ m^{-3}$ (Figure 3(a2)). Lower initial concentration (C_0), reduced primary emission (EMIS), enhanced wet scavenging (WETP), weakened aerosol chemical production (AERC), and weak-

https://doi.org/10.1021/acs.estlett.3c00490
Environ. Sci. Technol. Lett. 2023, 10, 779−785

ened cloud chemical production (CLDC) resulted in $PM_{2.5}$ decreases by 29.7 $\mu g\ m^{-3}$ (Figure 3(b2)), 203.2 $\mu g\ m^{-3}$ (Figure 3(c2)), 0.8 $\mu g\ m^{-3}$ (Figure 3(f2)), 21.3 $\mu g\ m^{-3}$ (Figure 3(g2)), and 5.0 $\mu g\ m^{-3}$ (Figure 3(h2)), respectively. On the contrary, weakened advection (ADVE) dilution, followed by weakened vertical mixing (VMIX) dilution, brought about $PM_{2.5}$ increases. ADVE and VMIX led to $PM_{2.5}$ increases of 256.9 $\mu g\ m^{-3}$ (Figure 3(d2)) and 13.1 $\mu g\ m^{-3}$ (Figure 3(e2)), respectively. As shown in Figure S11, the lower wind speed over the northern NCP was unbeneficial to transport and dilute aerosol particles, leading to local accumulation of $PM_{2.5}$. Meanwhile, according to simulation results of meteorology-driven process contribution changes (sensitivity experiments with fixed anthropogenic emissions but meteorology conditions change from the pre-lockdown level to lockdown level, Table S5), weakened ADVE was also diagnosed as the dominant factor for the increased $PM_{2.5}$ over the northern NCP during the lockdown period (Figure S12). Therefore, the $PM_{2.5}$ increase over the northern NCP during lockdown was primarily attributed to a weakened advection process induced by decreased wind speed.

We also noticed the significant discrepancy of $PM_{2.5}$ changes induced by the AERC process between the southern versus northern NCP. Benefiting from emission reduction of precursors, the $PM_{2.5}$ concentration contributed by the AERC process (AERC-$PM_{2.5}$ for short) decreased significantly ($-669.8\ \mu g\ m^{-3}$) over the southern NCP from pre-lockdown to lockdown. However, a much smaller decrease ($-21.3\ \mu g\ m^{-3}$) in the AERC-$PM_{2.5}$ concentration was found over the northern NCP; AERC-sulfate only decreased by 12.3 $\mu g\ m^{-3}$ (11.8%), and AERC-nitrate even increased by 5.4 $\mu g\ m^{-3}$ (4.1%). Here we took AERC-nitrate, which exhibited an unexpected increase in response to NO_x emission reduction, for further analysis. As shown in Figure 4, although NO_x emission was also largely reduced (by 30.6%) over the northern NCP from pre-lockdown to lockdown, the conversion rates of gas-phase reactions of OH with NO_2 and N_2O_5 to generate HNO_3 increased by 21.2%, and the heterogeneous reaction of N_2O_5 on the particle surface to generate nitrate increased by 370.5%. It was noted that HNO_3 formed by gas-phase reactions of OH with NO_2 and N_2O_5 were further converted to particulate nitrate, which was also included in the AERC process. The impact of elevated chemical conversion rates offset that of reduced NO_x emissions, eventually resulting in an unexpected increase in nitrate concentration (by 4.1%). Compared with pre-lockdown, the lockdown period experienced a higher daytime temperature (+2.7 K), higher nighttime relative humidity (+2.2%), and higher daily HO_x ($OH + HO_2$) concentration (+0.3 ppt) over the northern NCP, all of which were beneficial to promote chemical conversion efficiency and chemical formation of nitrate.

Limitation and Implication. It is noted that the formation of secondary organic aerosol (SOA) is not included in WRF-Chem with the CBMZ/MOSAIC scheme because CBMZ is hard-wired with a numerical solver and SOA condensable precursors cannot be directly added into it.[16,27,28] The lack of SOA simulation can lead to an underestimation of $PM_{2.5}$ and may cause uncertainty associated with the role of chemistry. However, $PM_{2.5}$ composition measurements over northern NCP showed that the ratio of organic in $PM_{2.5}$ decreased a lot, while the ratio of SIA (secondary inorganic aerosol, SIA = $SO_4^{2-} + NO_3^- + NH_4^+$) increased a lot from before to during the COVID-19 lockdown period,[29,36] indicating the greater impacts of SIA. Therefore, the uncertainty brought by SOA will not overturn the conclusion of present study. The impacts of the SOA will be discussed in our future study. Implication of the IPR method analyzed in this study is far beyond application to the COVID-19 air quality study. The improved method can be applied to any two periods and quantifies process contributions to changes in pollutant concentrations between the two periods. Since 2013, strict pollution control measures have been implemented to improve China's air quality. From 2013 to 2020, national $PM_{2.5}$ concentration has decreased by 48%, while ozone increased by 17%.[30] Although previous studies have examined the impacts of anthropogenic emissions and meteorological conditions on $PM_{2.5}$ decreases or ozone increases,[31−34] applying improved IPR analysis to year 2013 and year 2020 provides a novel process-level quantification perspective to explain pollutant changes.

■ ASSOCIATED CONTENT

Data Availability Statement

Meteorological measurements can be obtained from Wyoming Weather Web (http://weather.uwyo.edu/surface/meteorogram/seasia.shtml). Observed $PM_{2.5}$, O_3, and NO_2 concentrations can be accessed publicly from China National Environmental Monitoring Centre (https://quotsoft.net/air/).

Supporting Information

The Supporting Information is available free of charge at https://pubs.acs.org/doi/10.1021/acs.estlett.3c00490.

Model configuration (Text S1 and Table S1). Specific improvement steps for the improved IPR method (Text S2). Comparison of the differences in application between the traditional IPR method and improved IPR method (Text S3 and Figure S2). Model evaluation between observations and simulations (Text S4, Figures S3 to S10, Tables S2 to S4). Spatial distributions of changes in anthropogenic emissions (Figure S1). Changes in near surface wind speed (Figure S11). Meteorology-driven $PM_{2.5}$ changes and process contributions (Figure S12 and Table S5) (PDF)

■ AUTHOR INFORMATION

Corresponding Author

Hong Liao − *Jiangsu Key Laboratory of Atmospheric Environment Monitoring and Pollution Control, Jiangsu Collaborative Innovation Center of Atmospheric Environment and Equipment Technology, School of Environmental Science and Engineering, Nanjing University of Information Science and Technology, Nanjing 210044, China;* orcid.org/0000-0001-6628-1798; Email: hongliao@nuist.edu.cn

Authors

Lei Chen − *Jiangsu Key Laboratory of Atmospheric Environment Monitoring and Pollution Control, Jiangsu Collaborative Innovation Center of Atmospheric Environment and Equipment Technology, School of Environmental Science and Engineering, Nanjing University of Information Science and Technology, Nanjing 210044, China; State Environmental Protection Key Laboratory of Sources and Control of Air Pollution Complex, Beijing 100084, China; State Key Laboratory of Atmospheric Boundary Layer Physics and Atmospheric Chemistry, Institute of Atmospheric Physics Chinese Academy of Sciences, Beijing 100029, China*

https://doi.org/10.1021/acs.estlett.3c00490
Environ. Sci. Technol. Lett. 2023, 10, 779−785

Ke Li − *Jiangsu Key Laboratory of Atmospheric Environment Monitoring and Pollution Control, Jiangsu Collaborative Innovation Center of Atmospheric Environment and Equipment Technology, School of Environmental Science and Engineering, Nanjing University of Information Science and Technology, Nanjing 210044, China;* orcid.org/0000-0002-9181-3562

Jia Zhu − *Jiangsu Key Laboratory of Atmospheric Environment Monitoring and Pollution Control, Jiangsu Collaborative Innovation Center of Atmospheric Environment and Equipment Technology, School of Environmental Science and Engineering, Nanjing University of Information Science and Technology, Nanjing 210044, China*

Ziyu Long − *Jiangsu Key Laboratory of Atmospheric Environment Monitoring and Pollution Control, Jiangsu Collaborative Innovation Center of Atmospheric Environment and Equipment Technology, School of Environmental Science and Engineering, Nanjing University of Information Science and Technology, Nanjing 210044, China*

Xu Yue − *Jiangsu Key Laboratory of Atmospheric Environment Monitoring and Pollution Control, Jiangsu Collaborative Innovation Center of Atmospheric Environment and Equipment Technology, School of Environmental Science and Engineering, Nanjing University of Information Science and Technology, Nanjing 210044, China;* orcid.org/0000-0002-8861-8192

Yang Yang − *Jiangsu Key Laboratory of Atmospheric Environment Monitoring and Pollution Control, Jiangsu Collaborative Innovation Center of Atmospheric Environment and Equipment Technology, School of Environmental Science and Engineering, Nanjing University of Information Science and Technology, Nanjing 210044, China;* orcid.org/0000-0002-9008-5137

Meigen Zhang − *State Key Laboratory of Atmospheric Boundary Layer Physics and Atmospheric Chemistry, Institute of Atmospheric Physics Chinese Academy of Sciences, Beijing 100029, China; University of Chinese Academy of Sciences, Beijing 100049, China*

Complete contact information is available at: https://pubs.acs.org/10.1021/acs.estlett.3c00490

Author Contributions

H.L. designed the study. L.C. wrote the original manuscript. L.C., K.L. and J.Z. performed the research. Z.L., X.Y., Y.Y., and M.Z. discussed the results. All authors commented on the manuscript.

Notes

The authors declare no competing financial interest.

■ ACKNOWLEDGMENTS

This work is supported by National Key R&D Program of China (Grant 2022YFE0136100), National Natural Science Foundation of China (Grant 42305121, 42007195), University Natural Science Research Foundation of Jiangsu Province (Grant 21KJB170004), State Environmental Protection Key Laboratory of Sources and Control of Air Pollution Complex (Grant SCAPC202114), State Key Laboratory of Atmospheric Boundary Layer Physics and Atmospheric Chemistry (Grant LAPC-KF-2022-05), National Key R&D Program of China (Grant 2019YFA0606804), and Natural Science Foundation of Jiangsu Province (Grant BK20220031).

■ REFERENCES

(1) Bauwens, M.; Compernolle, S.; Stavrakou, T.; Muller, J. F.; van Gent, J.; Eskes, H.; Levelt, P. F.; van der, A. R.; Veefkind, J. P.; Vlietinck, J.; Yu, H.; Zehner, C. Impact of coronavirus outbreak on NO_2 pollution assessed using TROPOMI and OMI observations. *Geophysical Research Letters* **2020**, *47* (11), No. e2020GL087978.

(2) Shi, X.; Brasseur, G. P. The response in air quality to the reduction of Chinese economic activities during the COVID-19 outbreak. *Geophys. Res. Lett.* **2020**, *47*, No. e2020GL088070.

(3) Qiu, Y.; Ma, Z.; Li, K.; Lin, W.; Tang, Y.; Dong, F.; Liao, H. Markedly enhanced levels of peroxyacetyl nitrate (PAN) during COVID-19 in Beijing. *Geophys. Res. Lett.* **2020**, *47*, No. e2020GL089623.

(4) Field, R. D.; Hickman, J. E.; Geogdzhayev, I. V.; Tsigaridis, K.; Bauer, S. E. Changes in satellite retrievals of atmospheric composition over eastern China during the 2020 COVID-19 lockdowns. *Atmospheric Chemistry and Physics* **2021**, *21* (24), 18333−18350.

(5) Gao, M.; Zhou, Q.; Yang, X.; Li, Q.; Zhang, S.; Yung, K. L. L.; Guo, Y. Nonlinear modulation of COVID-19 transmission by climate conditions. *Meteorological Applications* **2021**, *28*, No. e1985.

(6) Wang, X.; Zhang, R. How did air pollution change during the COVID-19 outbreak in China? *Bulletin of the American Meteorological Society* **2020**, *101* (10), E1645−E1652.

(7) Huang, X.; Ding, A.; Gao, J.; Zheng, B.; Zhou, D.; Qi, X.; Tang, R.; Wang, J.; Ren, C.; Nie, W.; Chi, X.; Xu, Z.; Chen, L.; Li, Y.; Che, F.; Pang, N.; Wang, H.; Tong, D.; Qin, W.; Cheng, W.; Liu, W.; Fu, Q.; Liu, B.; Chai, F.; Davis, S. J.; Zhang, Q.; He, K. Enhanced secondary pollution offset reduction of primary emissions during COVID-19 lockdown in China. *National Science Review* **2021**, *8* (2), nwaa137.

(8) Wang, P.; Chen, K.; Zhu, S.; Wang, P.; Zhang, H. Severe air pollution events not avoided by reduced anthropogenic activities during COVID-19 outbreak. *Resources, Conservation, and Recycling* **2020**, *158*, 104814.

(9) Zhang, Y.; Ma, Z.; Gao, Y.; Zhang, M. Impacts of the meteorological condition versus emissions reduction on the $PM_{2.5}$ concentration over Beijing−Tianjin−Hebei during the COVID-19 lockdown. *Atmospheric and Oceanic Science Letters* **2021**, *14* (4), 100014.

(10) Le, T.; Wang, Y.; Liu, L.; Yang, J.; Yung, Y. L.; Li, G.; Seinfeld, J. H. Unexpected air pollution with marked emission reductions during the COVID-19 outbreak in China. *Science* **2020**, *369* (6504), 702−706.

(11) Huang, Z.; Ou, J.; Zheng, J.; Yuan, Z.; Yin, S.; Chen, D.; Tan, H. Process contributions to secondary inorganic aerosols during typical pollution episodes over the Pearl River Delta Region, China. *Aerosol and Air Quality Research* **2016**, *16*, 2129−2144.

(12) Zhang, Q.; Xue, D.; Liu, X.; Gong, X.; Gao, H. Process analysis of $PM_{2.5}$ pollution events in a coastal city of China using CMAQ. *Journal of Environmental Science* **2019**, *79*, 225−238.

(13) Gipson, G. L. Chapter 16: Process Analysis; *Science Algorithms of the EPA Models-3 Community Multiscale Air Quality (CMAQ) Modeling System*; EPA/600/R-99/030 (NTIS PB2000-100561); U.S. Environ. Prot. Agency: Washington DC, USA, 1999; 16-116-20.

(14) Li, L.; Huang, C.; Huang, H. Y.; Wang, Y. J.; Yan, R. S.; Zhang, G. F.; Zhou, M.; Lou, S. R.; Tao, S. K.; Wang, H. L.; Qiao, L. P.; Chen, C. H.; Streets, D. G.; Fu, J. S. An integrated process rate analysis of a regional fine particulate matter episode over Yangtze River Delta in 2010. *Atmos. Environ.* **2014**, *91*, 60−70.

(15) Tang, G.; Zhu, X.; Xin, J.; Hu, B.; Song, T.; Sun, Y.; Zhang, J.; Wang, L.; Cheng, M.; Chao, N.; Kong, L.; Li, X.; Wang, Y. Modelling study of boundary-layer ozone over northern China-Part I: Ozone budget in summer. *Atmospheric Research* **2017**, *187*, 128−137.

(16) Chen, L.; Zhu, J.; Liao, H.; Gao, Y.; Qiu, Y.; Zhang, M.; Liu, Z.; Li, N.; Wang, Y. Assessing the formation and evolution mechanisms of severe haze pollution in the Beijing−Tianjin−Hebei region using process analysis. *Atmospheric Chemistry and Physics* **2019**, *19* (16), 10845−10864.

(17) Li, J.; Han, Z.; Wu, Y.; Xiong, Z.; Xia, X.; Li, J.; Liang, L.; Zhang, R. Aerosol radiative effects and feedbacks on boundary layer meteorology and $PM_{2.5}$ chemical components during winter haze events over the Beijing-Tianjin-Hebei region. *Atmospheric Chemistry and Physics* **2020**, *20* (14), 8659−8690.
(18) Yang, H.; Chen, L.; Liao, H.; Zhu, J.; Wang, W.; Li, X. Impacts of aerosol−photolysis interaction and aerosol−radiation feedback on surface-layer ozone in North China during multi-pollutant air pollution episodes. *Atmospheric Chemistry and Physics* **2022**, *22* (6), 4101−4116.
(19) Zheng, B.; Zhang, Q.; Geng, G. N.; Chen, C. H.; Shi, Q. R.; Cui, M. S.; Lei, Y.; He, K. B. Changes in China anthropogenic emissions and air quality during the COVID-19 pandemic in 2020. *Earth System Science Data* **2021**, *13*, 2895−2907.
(20) Tao, W.; Liu, J.; Ban-Weiss, G. A.; Hauglustaine, D. A.; Zhang, L.; Zhang, Q.; Cheng, Y.; Yu, Y.; Tao, S. Effects of urban land expansion on the regional meteorology and air quality of eastern China. *Atmospheric Chemistry and Physics* **2015**, *15*, 8597−8614.
(21) Gao, J.; Zhu, B.; Xiao, H.; Kang, H.; Pan, C.; Wang, D.; Wang, H. Effects of black carbon and boundary layer interaction on surface ozone in Nanjing, China. *Atmospheric Chemistry and Physics* **2018**, *18*, 7081−7094.
(22) Cao, L.; Li, S.; Gu, Y.; Luo, Y. A three-dimensional simulation and process analysis of tropospheric ozone depletion events (ODEs) during the springtime in the Arctic using CMAQ. *Atmospheric Chemistry and Physics* **2023**, *23*, 3363−3382.
(23) Hu, W.; Zhao, Y.; Zhao, T.; Bai, Y.; Zhao, C.; Kong, S.; Chen, L.; Du, Q.; Zheng, H.; Lu, W.; Liu, W.; Sun, X. Aggravated chemical production of aerosols by regional transport and basin terrain in a heavy $PM_{2.5}$ pollution episode over central China. *Atmos. Environ.* **2023**, *294*, 119489.
(24) Liu, H.; Han, X.; Tang, G.; Zhang, J.; Xia, X.; Zhang, M.; Meng, L. Model analysis of vertical exchange of boundary layer ozone and its impact on surface air quality over the North China Plain. *Sci. Total Environ.* **2022**, *821*, 153436.
(25) Yang, X.; Wu, K.; Wang, H.; Liu, Y.; Gu, S.; Lu, Y.; Zhang, X.; Hu, Y.; Ou, Y.; Wang, S.; Wang, Z. Summertime ozone pollution in Sichuan Basin, China: Meteorological conditions, sources and process analysis,. *Atmos. Environ.* **2020**, *226*, 117392.
(26) Ye, F.; Rupakheti, D.; Huang, L.; T, N.; Kumar Mk, S.; Li, L.; Kt, V.; Hu, J. Integrated process analysis retrieval of changes in ground-level ozone and fine particulate matter during the COVID-19 outbreak in the coastal city of Kannur, India. *Environ. Pollut.* **2022**, *307*, 119468.
(27) Zhang, Y.; Chen, Y.; Sarwar, G.; Schere, K. Impact of gas-phase mechanisms on Weather Research Forecasting Model with Chemistry (WRF/Chem) predictions: Mechanism implementation and comparative evaluation. *Journal of Geophysical Research: Atmospheres* **2012**, *117*, D01301.
(28) Gao, M.; Carmichael, G. R.; Wang, Y.; Saide, P. E.; Yu, M.; Xin, J.; Liu, Z.; Wang, Z. Modeling study of the 2010 regional haze event in the North China Plain. *Atmospheric Chemistry and Physics* **2016**, *16*, 1673−1691.
(29) Sun, Y.; Lei, L.; Zhou, W.; Chen, C.; He, Y.; Sun, J.; Li, Z.; Xu, W.; Wang, Q.; Ji, D.; Fu, P.; Wang, Z.; Worsnop, D. R. A chemical cocktail during the COVID-19 outbreak in Beijing, China: Insights from six-year aerosol particle composition measurements during the Chinese New Year holiday. *Sci. Total Environ.* **2020**, *742*, 140739.
(30) Xiao, Q.; Geng, G.; Xue, T.; Liu, S.; Cai, C.; He, K.; Zhang, Q. Tracking $PM_{2.5}$ and O_3 pollution and the related health burden in China 2013−2020. *Environ. Sci. Technol.* **2022**, *56* (11), 6922−6932.
(31) Zhai, S.; Jacob, D. J.; Wang, X.; Shen, L.; Li, K.; Zhang, Y.; Gui, K.; Zhao, T.; Liao, H. Fine particulate matter ($PM_{2.5}$) trends in China, 2013−2018: separating contributions from anthropogenic emissions and meteorology. *Atmospheric Chemistry and Physics* **2019**, *19* (16), 11031−11041.
(32) Gao, Y.; Zhang, L.; Zhang, G.; Yan, F.; Zhang, S.; Sheng, L.; Li, J.; Wang, M.; Wu, S.; Fu, J. S.; Yao, X.; Gao, H. The climate impact on atmospheric stagnation and capability of stagnation indices in elucidating the haze events over North China Plain and Northeast China. *Chemosphere* **2020**, *258*, 127335.
(33) Li, K.; Jacob, D. J.; Shen, L.; Lu, X.; De Smedt, I.; Liao, H. Increases in surface ozone pollution in China from 2013 to 2019: anthropogenic and meteorological influences. *Atmospheric Chemistry and Physics* **2020**, *20*, 11423−11433.
(34) Zhang, M.; Zhao, C.; Yang, Y.; Du, Q.; Shen, Y.; Lin, S.; Gu, D.; Su, W.; Liu, C. Modeling sensitivities of BVOCs to different versions of MEGAN emission schemes in WRF-Chem (v3.6) and its impacts over eastern China. *Geoscientific Model Development* **2021**, *14*, 6155−6175.
(35) Liu, Y. C.; Ni, S. Y.; Jiang, T.; Xing, S. B.; Zhang, Y. S.; Bao, X. L.; Feng, Z. M.; Fan, X. L.; Zhang, L.; Feng, H. B. Influence of Chinese New Year overlapping COVID-19 lockdown on HONO sources in Shijiazhuang. *Sci. Total Environ.* **2020**, *745*, 141025.
(36) Sun, Y.; Lei, L.; Zhou, W.; Chen, C.; He, Y.; Sun, J.; Li, Z.; Xu, W.; Wang, Q.; Ji, D.; Fu, P.; Wang, Z.; Worsnop, D. R. A chemical cocktail during the COVID-19 outbreak in Beijing, China: Insights from six-year aerosol particle composition measurements during the Chinese New Year holiday. *Sci. Total Environ.* **2020**, *742*, 140739.
(37) Li, R.; Zhao, Y. L.; Fu, H. B.; Chen, J. M.; Peng, M.; Wang, C. Y. Substantial changes in gaseous pollutants and chemical compositions in fine particles in the North China Plain during the COVID-19 lockdown period: anthropogenic vs. meteorological influences. *Atmospheric Chemistry and Physics* **2021**, *21*, 8677−8692.
(38) Meng, J. J.; Li, Z.; Zhou, R. W.; Chen, M.; Li, Y. Y.; Yi, Y. N.; Ding, Z. J.; Li, H. J.; Yan, L.; Hou, Z. F.; Wang, G. H. Enhanced photochemical formation of secondary organic aerosols during the COVID-19 lockdown in Northern China. *Sci. Total Environ.* **2021**, *758*, 143709.
(39) Yang, J. R.; Wang, S. B.; Zhang, R. Q.; Yin, S. S. Elevated particle acidity enhanced the sulfate formation during the COVID-19 pandemic in Zhengzhou, China. *Environ. Pollut.* **2022**, *296*, 118716.
(40) Hua, N.; Shang, Y.; Xie, M. J. Variations in $PM_{2.5}$ composition and sources during 2020−2021 COVID-19 epidemic periods in Nanjing. *Environmental Science* **2023**, *44* (2), 593−601.
(41) Dai, Q.; Liu, B.; Bi, X.; Wu, J.; Liang, D.; Zhang, Y.; Feng, Y.; Hopke, P. K. Dispersion Normalized PMF Provides Insights into the Significant Changes in Source Contributions to $PM_{2.5}$ after the COVID-19 Outbreak. *Environ. Sci. Technol.* **2020**, *54*, 9917−9927.
(42) Ren, C.; Huang, X.; Wang, Z.; Sun, P.; Chi, X.; Ma, Y.; Zhou, D.; Huang, J.; Xie, Y.; Gao, J.; Ding, A. Nonlinear response of nitrate to NO_x reduction in China during the COVID-19 pandemic. *Atmos. Environ.* **2021**, *264*, 118715.

https://doi.org/10.1021/acs.estlett.3c00490
Environ. Sci. Technol. Lett. 2023, 10, 779−785